MOLECULAR PHYSICS, 10–20 DECEMBER 2004, VOL. 102, NO. 23–24, 2451–2466

Taylor & Francis
Taylor & Francis Group

Electronic structure of vanadium and chromium carbide cations, VC^+ and CrC^+. Ground and low-lying states

IOANNIS S. K. KERKINES and ARISTIDES MAVRIDIS*

Laboratory of Physical Chemistry, Department of Chemistry, National and Kapodistrian University of Athens, P.O. Box 64 004, 157 10 Zografou, Athens, Greece

(*Received 13 May 2004; accepted 21 June 2004*)

The ground and low-lying states of the monopositive vanadium and chromium carbides, VC^+ and CrC^+ have been studied by multireference methods and quantitative basis sets. Potential energy curves for 17 (VC^+) and 19 (CrC^+) states have been fully calculated. A variety of binding modes is revealed in the low-lying spectrum of the two molecular cations, often accompanied with an electronic charge transfer from the metal cation towards carbon. Two states compete for the ground state identity in both systems. One state comprises two π and $\frac{1}{2}\sigma$ bonds (similarly to ScC^+ and TiC^+), while the other state forms a genuine triple bond. After a rather intricate analysis including core electron effects, scalar relativity and curve shifts, the formal ground states of VC^+ and CrC^+ are found to be of $^3\Delta$ and $^2\Delta$ symmetry, with estimated energy differences from the competing $^1\Sigma^+$ and $^4\Sigma^-$ states of 1–3 and 3–7 kcal/mol, respectively. At the highest level of theory including core/valence correlation and one-electron relativistic effects, the calculated ground-state binding energies are in satisfactory agreement with available experimental values.

1. Introduction

The transition metal–carbon bond plays a fundamental rôle in many chemical processes and reactions. The determination of its nature, even in small molecules, remains a challenge [1]. Most experimental work on the, simplest, diatomic transition metal carbides has been focused on species of the 2nd and 3rd transition metal rows [2]. The literature on the corresponding species of the 1st transition metal row is surprisingly scarce [3], and for their monocationic counterparts, even scarcer. For the cations MC^+, where M=Sc, Ti, ...,Cu, the only experimental information available are the dissociation energies of the (unknown symmetry) ground states of ScC^+ [4], TiC^+ [4], VC^+ [5], CrC^+ [6], FeC^+ [7], and CoC^+ [7, 8]. Theoretically, and with the help of highly correlated multireference calculations, the symmetries of the ground states of MC^+ (M=Sc, Ti, V, Cr, Fe) have been established [9–11] and several low-lying states have been studied for the ScC^+, TiC^+, and FeC^+ moieties [10, 11]. Older theoretical work by Harrison [12] was focused on the $^4\Sigma^-$ and $^4\Pi$ states of CrC^+ employing multireference configuration interaction methods coupled with double zeta + P quality basis sets. Recently, Gutsev *et al.* [13] attempted to predict the ground states of the entire first-row transition metal MC^+ series using the density functional approach (BLYP, B3LYP, BPW91). These authors also predict a $^4\Sigma^-$ ground state for CrC^+ at the B3LYP and BPW91 levels of theory, but at the BLYP level they find a $^2\Delta$ ground state [13]. Supported by our large multireference configuration interaction (MRCI) results including relativistic contributions as well as the effect of the $3s^23p^6$ 'core' electrons of the transition metal, we have already pointed out that the ground state of CrC^+ is of $^2\Delta$ symmetry [9]. For the VC^+ cation, the density-functional theory (DFT) results of Gutsev *et al.* suggest that the ground state is $^3\Delta$ [13]. Our large MRCI calculations have indicated however, that, although formally the ground state of VC^+ is of $^3\Delta$ symmetry [9], the situation is more involved due to a similar to CrC^+ (and maybe even 'fiercer') competition between the $^3\Delta$ and $^1\Sigma^+$ states (*vide infra*).

To obtain reliable spectroscopic parameters, as well as to interpret the bonding nature in their low-lying states, we have performed complete active space self-consistent field + singles + doubles configuration interaction (CASSCF + 1 + 2 = MRCI) calculations on the VC^+ and CrC^+ molecular cations; the present study can be viewed as a continuation of our work on ScC^+, TiC^+ [10] and FeC^+ [11].

The lowest-lying dissociation channels of the VC^+ cation in ascending energy order are $V^+(3d^4, a\,^5D) + C(^3P)$, $V^+(4s^13d^3, a\,^5F) + C(^3P)$, and $V^+(4s^13d^3, a\,^3F) + C(^3P)$,

*Author for correspondence. e-mail: mavridis@chem.uoa.gr

Molecular Physics ISSN 0026–8976 print/ISSN 1362–3028 online © 2004 Taylor & Francis Ltd
http://www.tandf.co.uk/journals
DOI: 10.1080/00268970420002749 64

while for CrC^+ they are $Cr^+(3d^5,\ a\ ^6S) + C(^3P)$, $Cr^+(3d^5,\ a\ ^6S) + C(^1D)$, $Cr^+(4s^13d^4,\ a\ ^6D) + C(^3P)$, $Cr^+(4s^13d^4,\ a\ ^4D) + C(^3P)$, and $Cr^+(3d^5,\ a\ ^4G) + C(^3P)$ [16]. Table 1 collects the relevant theoretical and experimental atomic energy splittings among the lowest lying states of V^+, Cr^+, and C. We note that, (a) the ground state term of $V^+(a\ ^5D)$ is predicted to be the same as the experimental one [16], only after dynamical correlation is taken into account (i.e. at the MRCI level); (b) the rather inadequate description of the first excited term of $Cr^+(a\ ^6D)$ at the spherically averaged SCF level (= CASSCF in this case) places the $Cr^+(4s^13d^4,\ a\ ^6D) + C(^3P)$ asymptotic channel lower than $Cr^+(3d^5,\ a\ ^6S) + C(^1D)$, contrary to experiment [16]. In both cases, this 'deficiency' of the reference CASSCF calculations caused problems of technical nature, which were more severe in the calculation of several excited states of CrC^+.

The aforementioned lowest-lying asymptotic channels engender 99 and 108 molecular $^{2S+1}|\Lambda|$ states for VC^+ (of $\Sigma^\pm$, Π, Δ, Φ, and Γ symmetry, S = 0, 1, 2, and 3) and CrC^+ (of $\Sigma^\pm$, Π, Δ, Φ, Γ, and H symmetry, S = 1/2, 3/2, 5/2, and 7/2), respectively. Out of preliminary CASSCF calculations for all these states, 17(VC^+) and 19(CrC^+) were selected to be investigated more thoroughly at the MRCI level, employing the arbitrary criterion of being the lowest in energy at the CASSCF level of theory.

For almost all states studied in the present work we report total energies, dissociation energies (D_e), bond distances (r_e), harmonic (ω_e) and anharmonic ($\omega_e x_e$) frequencies, Mulliken charges and energy gaps (T_e), as well as full potential energy curves (PECs). PECs are crucial for a better understanding of bonding evolution along the interaction path and for correct identification of the *in situ* atomic characters. The fundamental necessity of the latter will be unveiled shortly in a rather 'dramatic' way while attempting to clarify the ground state identities for both VC^+ and CrC^+ (*vide infra*).

2. Technical details

For the V and Cr atoms the Atomic Natural Orbital (ANO) Gaussian basis sets 20s15p10d6f4g of Bauschlicher [17] were employed. For the carbon atom the correlation-consistent basis set of quadruple-ζ quality, i.e. 12s6p3d2f1g of Dunning [18] was used. Both sets were generally contracted to [7s6p4d3f2g/5s4p3d2f1g], thus the one-electron basis set space consists of 139 spherical Gaussian functions (5d, 7f and 9g). The effect of one 11-component h (l = 5; exponent = 1.0) function to the D_e and r_e values of the two lowest-lying states of CrC^+ was also examined. The adequacy of these one-electron bases was further supported by the small basis set superposition error (BSSE) estimates [19] of 0.16 and 0.34 kcal mol^{-1} at the ground state equilibrium geometries of VC^+ and CrC^+. For correlated calculations including the $3s^23p^6$ core electrons of the transition metal atoms (C-MRCI), the same ANO basis sets were used. The effects of relativity for the lowest-lying states of both VC^+ and CrC^+ were examined at the MRCI level through the one-electron Douglas-Kroll (DK) approximation [20], using the same ANO (but uncontracted now) basis sets for V and Cr, and the DK-recontracted cc-pVQZ basis set for C [21].

The CASSCF reference space for both molecules studied comprises 10 orbital functions, correlating asymptotically to the 'valence' (occupied) spaces of the $M^+(4s + 3d)$ and $C(2s + 2p)$ atoms. Considering the $1s^22s^22p^63s^23p^6$ and $1s^2$ electrons of V^+ or Cr^+ and C atoms respectively as 'core' (inactive), our reference space is defined by distributing eight or nine e^- among the ten 'valence' orbitals. For the ground states, the reference space consists of 5196 (VC^+) and 6996 (CrC^+) CFs (configuration functions). The CASSCF wave functions (but not the MRCI ones) display pure axial angular momentum symmetry (i.e. $|\lambda| = 0$, 1, 2, 3, 4 and 5 for $\Sigma^\pm$, Π, Δ, Φ, Γ, and H states, respectively), even though the calculations were performed within the C_{2v} point group. The largest MRCI expansion contains $\sim$66 000 000 CFs (ground state of CrC^+), which is very efficiently reduced to $\sim$1 200 000 through the internal contraction technique [22].

The presence of many low-lying excited molecular states of the same symmetry necessitates the use of the state-average (SA) [23] approach. Combined losses in total energy due to the SA approach and due to the size-nonextensivity errors in such systems are of the order of 2 to 3 mE_H with a synchronous bond length increase of 0.005–0.015 Å at the MRCI level of theory [24].

All our calculations were performed with the MOLPRO 2002 software package [25].

3. Results and discussion

In section 3.1 we discuss the VC^+ and in 3.2 the CrC^+ molecule. With the exception of the ground states marked *X*, in all other states a number in front of the molecular term symbol indicates the absolute energy ordering of the state with respect to the *X* state; a second number in parenthesis gives the ordering of the states within the same symmetry manifold.

3.1 *The VC^+ cation*

Table 2 presents our numerical results for all 17 computed states of the VC^+ cation, while table 3 gives the asymptotic descriptions $|V^+>|C>$, leading CASSCF equilibrium configurations, and CASSCF

Table 1. Energies E (hartree) and atomic energy splittings (eV) among the low lying states of V^+, Cr^+, and C in different methodologies (see the 'technical details' section for the basis sets used).

	V^+				Cr^+						C			
Method	$E(a\ ^5D)$	$a\ ^5F \leftarrow a\ ^5D$	$a\ ^3F \leftarrow a\ ^5D$	$a\ ^3P \leftarrow a\ ^5D$	$E(a\ ^6S)$	$a\ ^6D \leftarrow a\ ^6S$	$a\ ^4D \leftarrow a\ ^6S$	$a\ ^4G \leftarrow a\ ^6S$	$a\ ^4P \leftarrow a\ ^6S$	Method	E	$^1D \leftarrow {}^3P$	$^1S \leftarrow {}^3P$	$^5S \leftarrow {}^3P$
NHF[a]	−942.6707837				−1043.139393					NHF[a]	−37.688619			
sa-SCF[b]	−942.670316	−0.151	0.757	2.164	−1043.138834	1.153	2.254	3.264	3.754	sa-SCF[b]	−37.688234			
MRCI	−942.725278	0.381	1.069	1.607	−1043.224227	1.727	2.615	2.890	3.063	SA-CASSCF[g]	−37.705548	1.575	2.613	2.909
MRCI + Q[c]	−942.72636	0.398	1.067	1.455	−1043.22613	1.748	2.611	2.855	2.997	CISD	−37.783239	1.299	2.734	4.109
C-MRCI[d]	−943.037603	0.383	1.203	1.688	−1043.547969	1.622	2.634	2.776	3.013	MRCI	−37.784932	1.287	2.695	4.109
C-MRCI + Q[d]	−943.05942	0.432	1.204	1.574	−1043.57114	1.655	2.615	2.679	2.846	MRCI + Q[c]	−37.7879	1.27	2.70	4.18
C-MRCI(DK)[e]	−948.327371	0.129	0.982	1.658	−1049.88976	1.321	2.379	2.738	2.971	Experiment[f]		1.260	2.680	4.179
C-MRCI + Q(DK)[e]	−948.35195	0.176	0.979	1.532	−1049.9156	1.352	2.355	2.637	2.800					
Experiment[f]		0.337	1.078	1.426		1.522	2.458	2.544	2.706					

[a] Numerical Hartree-Fock, refs [14] and [15].
[b] Spherically averaged SCF.
[c] MRCI + multireference Davidson correction.
[d] The 'core' $3s^23p^6$ electrons were included in the correlation treatment.
[e] One-electron relativistic effects included via the Douglas-Kroll (DK) approximation.
[f] Averaged over M_J values, ref [16].
[g] State averaged CASSCF.

Table 2. Total energies E (hartree), dissociation energies D_e (kcal mol^{-1}), bond lengths, r_e (Å), harmonic and anharmonic frequencies ω_e, $\omega_e x_e$ (cm^{-1}), and energy gaps T_e(kcal mol^{-1}) of seventeen states of the VC^+ species at the MRCI[a] (MRCI + Q)[b] level of theory.

State[c]	$-E$	D_e[d]	r_e	ω_e	$\omega_e x_e$	T_e
$X\ ^3\Delta(1)$	980.633396	79.0	1.667	874	8.8	0.0
	(0.64080)	(79.4)	(1.67)	(863)	(8.3)	
$1\ ^1\Sigma^+(1)$	980.628530	100.1	1.576	952	6.7	3.1
	(0.63612)	(100.9)	(1.58)	(940)	(6.0)	(3.0)
$2\ ^1\Delta(1)$	980.619986	95.5	1.718	786	5.4	8.4
	(0.62803)	(96.4)	(1.72)	(782)	(6.0)	(8.0)
$3\ ^3\Phi(1)$	980.614169	66.9	1.739	783	8.0	12.1
	(0.62223)	(67.6)	(1.74)	(774)	(9.2)	(11.7)
$4\ ^3\Pi(1)$	980.614113	66.9	1.740	758	0.6	12.1
	(0.62223)	(67.6)	(1.75)	(751)	(4.2)	(11.7)
$5\ ^1\Phi(1)$	980.606165	86.7	1.740	775	3.0	17.1
	(0.61442)	(87.9)	(1.74)	(767)	(3.1)	(16.6)
$6\ ^5\Pi(1)$	980.598448	57.0	1.830	698	5.1	21.9
	(0.60809)	(58.7)	(1.83)	(692)	(5.0)	(20.5)
$7\ ^1\Pi(1)$	980.594029	79.4	1.791	635		24.7
	(0.60271)	(80.7)	(1.80)	(639)		(23.9)
$8\ ^5\Sigma^+(1)$	980.591909	53.1	1.891	683	4.0	26.0
	(0.60212)	(55.1)	(1.89)	(683)	(7.8)	(24.3)
$9\ ^3\Sigma^+(1)$	980.581777	46.8	1.915	661	3.8	32.4
	(0.59141)	(48.5)	(1.92)	(654)	(4.2)	(31.0)
$10\ ^7\Sigma^+(1)$	980.580465	45.8	2.001	637	3.2	33.2
	(0.58903)	(46.9)	(2.01)	(629)	(2.4)	(32.5)
$11\ ^5\Phi(1)$	980.579409	45.1	1.901	634	2.4	33.9
	(0.58875)	(46.6)	(1.91)	(622)	(1.5)	(32.7)
$12\ ^5\Delta(1)$	980.578749	44.9	1.928	667	13	34.3
	(0.58908)	(47.1)	(1.91)	(680)	(13)	(32.5)
$13\ ^3\Pi(2)$	980.575862	43.6	1.864	674	6.7	36.1
	(0.58532)	(45.1)	(1.87)	(657)	(3.4)	(34.8)
$14\ ^5\Pi(2)$	980.569902	39.9	1.864	685	5.2	39.8
	(0.57926)	(41.4)	(1.87)	(671)	(5.2)	(38.6)
$15\ ^7\Pi(1)$	980.569432	39.0	2.046	626	3.5	40.1
	(0.57959)	(41.1)	(2.04)	(618)	(3.4)	(38.4)
$16\ ^7\Phi(1)$	980.558946	32.5	2.075	608	3.3	46.7
	(0.56882)	(34.3)	(2.08)	(612)	(3.9)	(45.2)

[a]Internally contracted MRCI.
[b]'+Q' refers to the multireference Davidson correction.
[c]Numbers in parenthesis after the term symbol indicate the energy ordering within the same symmetry manifold.
[d]D_e with respect to the adiabatic products.

Mulliken atomic populations. Full potential energy curves for these states at the MRCI level are shown in figure 1.

Our recent MRCI calculations [9] have indicated that the $^3\Delta(1)$ and $^1\Sigma^+(1)$ states are candidates for the ground state of VC^+. At the MRCI level of theory, it was found that formally the ground state is the $^3\Delta(1)$, with the $^1\Sigma^+(1)$ being higher by about 3 kcal mol^{-1} [9]. For the $^3\Delta(1)$ state, the wavefunction composition in conjunction with the atomic Mulliken distributions suggest a binding mode depicted graphically with the following valence-bond-Lewis (vbL) icon [9]:

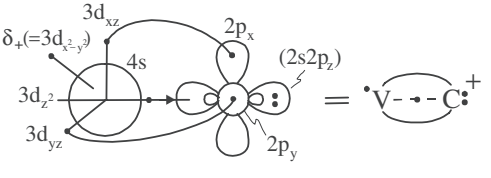

$V^+(3d^4, {}^5D; M = \pm 2)$ C (^3P; M = 0) $X\ ^3\Delta$ (1)

Table 3. Asymptotic fragments, leading equilibrium CASSCF CFs, and equilibrium CASSCF Mulliken atomic populations of seventeen VC^+ states.

State	Adiabatic fragments[a]	Dominant equilibrium CASSCF CFs	Equilibrium CASSCF Mulliken atomic populations										
			V							C			
			4s	$4p_\sigma$	$4p_\pi$	$3d_\sigma$	$3d_{xz}$	$3d_{yz}$	$3d_\delta$	2s	$2p_z$	$2p_x$	$2p_y$
X $^3\Delta(1)$	$\|\pm1\rangle\|\pm1\rangle$	$0.89\|1\sigma^2 2\sigma^1 1\pi_x^2 1\pi_y^2 1\delta^1\rangle$	0.09	0.06	0.04	0.61	1.05	1.05	1.0	1.73	0.53	0.90	0.90
1 $^1\Sigma^+(1)$	$\|\pm1\rangle\|\mp1\rangle^b$	$0.85\|1\sigma^2 2\sigma^2 1\pi_x^2 1\pi_y^2\rangle$	0.12	0.09	0.04	1.24	1.14	1.14	0.10	1.80	0.72	0.78	0.78
2 $^1\Delta(1)$	$\|\pm2\rangle\|0\rangle^b$	$0.85\|1\sigma^2 2\sigma^1 1\pi_x^2 1\pi_y^2 \overline{1\delta}^1\rangle$	0.10	0.06	0.04	0.46	1.11	1.11	1.0	1.66	0.73	0.84	0.84
3 $^3\Phi(1)$	$\|\pm2\rangle\|\pm1\rangle$	$0.61(\|1\sigma^2 2\sigma^2 1\pi_x^2 1\pi_y^1 1\delta_-^1\rangle + \|1\sigma^2 2\sigma^2 1\pi_x^1 1\pi_y^2 1\delta_+^1\rangle)^c$	0.11	0.09	0.04	1.09	0.78	0.78	1.04	1.80	0.88	0.69	0.69
4 $^3\Pi(1)$	$\|\pm1\rangle\|0\rangle$	$0.60(\|1\sigma^2 2\sigma^2 1\pi_x^2 1\pi_y^1 1\delta_-^1\rangle - \|1\sigma^2 2\sigma^2 1\pi_x^1 1\pi_y^2 1\delta_+^1\rangle)^c$	0.11	0.08	0.04	1.05	0.78	0.78	1.06	1.80	0.88	0.69	0.69
5 $^1\Phi(1)$	$\|\pm2\rangle\|\pm1\rangle^b$	$0.60(\|1\sigma^2 2\sigma^2 \overline{1\pi}_x^1 1\pi_y^2 1\delta_+^1\rangle + \|1\sigma^2 2\sigma^2 1\pi_x^2 1\pi_y^1 \overline{1\delta}_-^1\rangle)^c$	0.14	0.09	0.04	1.16	0.71	0.71	1.0	1.78	0.82	0.75	0.75
6 $^5\Pi(1)$	$\|\pm2\rangle\|\mp1\rangle$	$0.76\|1\sigma^2 2\sigma^1 1\pi_x^2 1\pi_y^1 1\delta_+^1 1\delta_-^1\rangle^c$	0.19	0.05	0.05	0.53	0.89	0.44	1.76	1.74	0.73	0.94	0.66
7 $^1\Pi(1)$	$\|\pm1\rangle\|0\rangle^b$	$0.50(\|1\sigma^2 2\sigma^2 \overline{1\pi}_x^1 1\pi_y^2 1\delta_+^1\rangle - \|1\sigma^2 2\sigma^2 1\pi_x^2 1\pi_y^1 \overline{1\delta}_-^1\rangle)^c$	0.14	0.09	0.04	0.97	0.79	0.79	1.22	1.75	0.82	0.78	0.78
8 $^5\Sigma^+(1)$	$\|0\rangle\|0\rangle$	$0.77\|1\sigma^2 2\sigma^2 1\pi_x^1 1\pi_y^1 1\delta_+^1 1\delta_-^1\rangle$	0.18	0.06	0.04	0.97	0.34	0.34	1.94	1.81	0.98	0.67	0.67
9 $^3\Sigma^+(1)$	$\|\pm1\rangle\|\mp1\rangle$	$0.53\|1\sigma^2 2\sigma^2 \overline{1\pi}_x^1 1\pi_y^1 1\delta_+^1 1\delta_-^1\rangle - 0.43\|1\sigma^2 2\sigma^2 1\pi_x^1 1\pi_y^1 1\delta_+^1 \overline{1\delta}_-^1\rangle$	0.14	0.10	0.04	1.07	0.33	0.33	1.84	1.78	0.90	0.73	0.73
10 $^7\Sigma^+(1)$	$\|\pm1\rangle\|\mp1\rangle$	$0.97\|1\sigma^2 2\sigma^1 3\sigma^1 1\pi_x^1 1\pi_y^1 1\delta_+^1 1\delta_-^1\rangle$	0.35	0.10	0.08	0.99	0.19	0.19	2.0	1.72	0.82	0.76	0.76
11 $^5\Phi(1)$	$\|\pm2\rangle\|\pm1\rangle$	$0.58(\|1\sigma^2 2\sigma^1 3\sigma^1 1\pi_x^2 1\pi_y^1 1\delta_-^1\rangle - \|1\sigma^2 2\sigma^1 3\sigma^1 1\pi_x^1 1\pi_y^2 1\delta_+^1\rangle)^c$	0.45	0.07	0.04	0.92	0.74	0.74	1.0	1.72	0.83	0.73	0.73
12 $^5\Delta(1)$	$\|\pm2\rangle\|0\rangle$	$0.60(\|1\sigma^2 2\sigma^1 1\pi_x^2 1\pi_y^1 2\pi_y^1 1\delta_+^1\rangle + \|1\sigma^2 2\sigma^1 1\pi_x^1 2\pi_x^1 1\pi_y^2 1\delta_+^1\rangle)^d$	0.18	0.06	0.06	0.36	1.06	1.06	1.0	1.68	0.73	0.89	0.89
13 $^3\Pi(2)$	$\|\pm2\rangle\|\mp1\rangle$	$0.54\|1\sigma^2 2\sigma^1 1\pi_x^2 1\pi_y^1 \overline{1\delta}_+^1 1\delta_-^1\rangle + 0.42\|1\sigma^2 2\sigma^1 1\pi_x^2 1\pi_y^1 1\delta_+^1 \overline{1\delta}_-^1\rangle^c$	0.11	0.07	0.05	0.46	0.97	0.40	1.82	1.70	0.81	0.90	0.67
14 $^5\Pi(2)$	$\|0\rangle\|\pm1\rangle$	$0.46\|1\sigma^2 2\sigma^1 1\pi_x^2 1\pi_y^1 1\delta_+^1 1\delta_-^1\rangle - 0.56(\|1\sigma^2 2\sigma^1 3\sigma^1 1\pi_x^2 1\pi_y^1 1\delta_-^1\rangle + \|1\sigma^2 2\sigma^1 3\sigma^1 1\pi_x^1 1\pi_y^2 1\delta_+^1\rangle)^c$	0.37	0.05	0.05	0.78	0.76	0.70	1.36	1.75	0.77	0.83	0.64
15 $^7\Pi(1)$	$\|\pm1\rangle\|0\rangle$	$0.77\|1\sigma^2 2\sigma^1 1\pi_x^1 2\pi_x^1 1\pi_y^1 1\delta_+^1 1\delta_-^1\rangle + 0.43(\|1\sigma^2 2\sigma^1 3\sigma^1 1\pi_x^1 2\pi_x^1 1\pi_y^1 1\delta_-^1\rangle - \|1\sigma^2 2\sigma^1 3\sigma^1 1\pi_x^1 1\pi_y^1 2\pi_y^1 1\delta_+^1\rangle)^c$	0.31	0.08	0.07	0.51	0.87	0.37	1.62	1.70	0.79	0.89	0.79
16 $^7\Phi(1)$	$\|\pm2\rangle\|\pm1\rangle$	$0.69(\|1\sigma^2 2\sigma^1 3\sigma^1 1\pi_x^1 2\pi_x^1 1\pi_y^1 1\delta_+^1\rangle + \|1\sigma^2 2\sigma^1 3\sigma^2 1\pi_x^1 1\pi_y^1 2\pi_y^1 1\delta_+^1\rangle)^c$	0.48	0.09	0.06	0.95	0.65	0.65	1.0	1.71	0.77	0.82	0.82

[a] $|V^+;{}^5D;M\rangle|C;{}^3P;M\rangle$.
[b] $|V^+;{}^3F;M\rangle|C;{}^3P;M\rangle$.
[c] B_1 symmetry component.
[d] A_1 symmetry component.

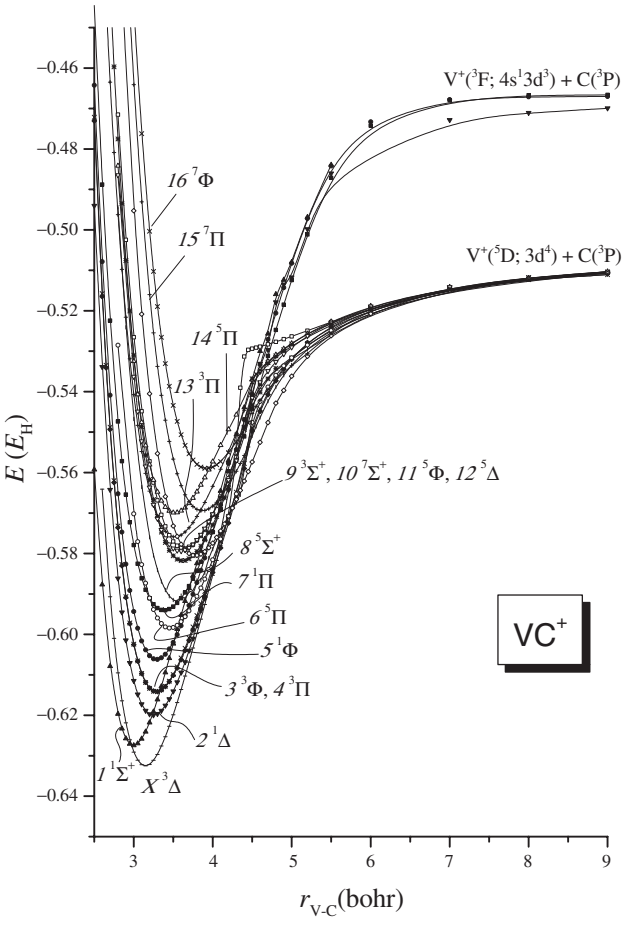

Figure 1. Potential energy curves of VC^+. MRCI level of theory.

The binding mode consists of 2π and 1/2 σ bonds and is identical to the one found in the ground $X\ ^2\Sigma^+$ state of TiC^+ [9–10]. The 'extra' electron is placed in an orbital of δ symmetry, just observing the chemical bond and defining the spatial symmetry. As a result, the binding energy (D_0) and bond length (r_e) of $VC^+(^3\Delta)$, 85.4 kcal mol^{-1} and 1.645 Å, at our best computational level, closely resemble those of TiC^+ ($X\ ^2\Sigma^+$ 93.5 kcal mol^{-1}, 1.662 Å) [9]. The experimental dissociating energy of the ground VC^+ state is $D_0 = 88.4 \pm 1.2$ kcal mol^{-1}, as obtained by guided ion-beam spectrometric techniques [5b].

The $^3\Delta(1)$ state differentiates its bonding character around 4.2 bohr due to an avoided crossing from $|a^5\mathrm{D};\ \mathrm{M} = \pm 1\rangle_{V^+} \otimes |^3\mathrm{P};\ \mathrm{M} = \pm 1\rangle_C$ at infinity to $|a^5\mathrm{D};\ \mathrm{M} = \pm 2\rangle_{V^+} \otimes |^3\mathrm{P};\ \mathrm{M} = 0\rangle_C$ near equilibrium, thus dissociating to the ground state fragments, $V^+(3d^4,\ a\ ^5D) + C(^3P)$. The situation in the $^1\Sigma^+$ (1) state, however, is much more involved. Starting at infinity from the excited $V^+(4s^13d^3,\ a\ ^3F) + C(^3P)$ asymptotic channel, the $^1\Sigma^+(1)$ state undergoes an avoided crossing with a $^1\Sigma^+$ state originating from an even higher excited channel, $V^+(3d^4,\ a\ ^3P) + C(^3P)$ approximately 1.5 eV above the ground state fragments (table 1). Due to the existence of two other excited dissociation channels lying in between, the calculation of the $^1\Sigma^+$ PEC at the MRCI (but not at the CASSCF) level to complete dissociation was not feasible. However, we were able to calculate the supermolecule, and therefore the binding energy of this state is, $D_e = 100.1$ kcal mol^{-1} with respect to the adiabatic fragments $V^+(a\ ^3F) + C(^3P)$; see table 2.

According to the results in table 3, the $^1\Sigma^+(1)$ state exhibits a formal triple bond, scheme 2.

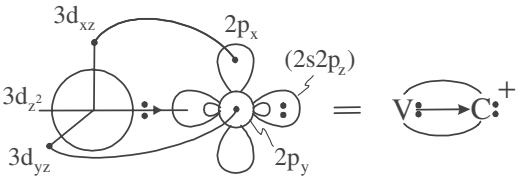

$V^+(3d^4, a\ ^3P;\ M = 0)$ $C\ (^3P;\ M = 0)$ $1\ ^1\Sigma^+$ (2)

Note that the *in situ* V^+ cation finds itself in its third excited state, $a\ ^3P$, with a $3d^4$ electron configuration.

Results from the competing $X\ ^3\Delta$ and $1\ ^1\Sigma^+$ states are shown in table 4. Including relativistic effects and core/valence contributions, the $^3\Delta(1)$ still remains the ground state, with a BSSE-free energy difference from the $^1\Sigma^+(1)$ state, T_0 $(= T_e - \Delta\omega_e/2) = 2.7$ (4.1) kcal mol^{-1} at the MRCI (MRCI + Q) level. However, since the $^1\Sigma^+(1)$ state originates from an excited $V^+ + C$ asymptote, care has to be exercised that the transition energy to this excited channel from the ground state fragments is taken into consideration. The situation is even subtler since we have to keep in mind that the *in situ* V^+ cation is in the $^3P(3d^4)$ and not in the $^3F(4s^13d^3)$ excited state, as a result of the aforementioned avoided crossing. At our best theoretical level, C-MRCI(DK)[C-MRCI(DK) + Q], the $^3P \leftarrow {}^5D$ energy gap is predicted higher than the experimental one by 5.35[2.44] kcal mol^{-1} (table 1). Assuming 'perfect' parallel shifting of the curves to match the experimental $^3P \leftarrow {}^5D$ splitting, final $T_0(^1\Sigma^+ - {}^3\Delta)$ values of −2.65 and +1.61 kcal mol^{-1} are obtained. Thus, at the C-MRCI(DK) level the ground state is of $^1\Sigma^+$ symmetry, while the C-MRCI(DK) + Q ground state has a $^3\Delta$ symmetry. Therefore, a rather unfortunate situation arises, i.e. highly correlated calculations including core/valence effects and relativistic contributions are unable to

pinpoint the ground state of a 'prosaic' diatomic system. Nevertheless, due to the rather approximate nature of the 'perfect' parallel curve shifting, and the fairly indicative Davidson-corrected T_0 values in the case when core electrons are correlated, we dare predict that the ground state of VC^+ is most probably of $^3\Delta$ symmetry. However, a careful and accurate experimental study is needed to resolve the ground state problem of this interesting diatomic cation.

The second excited state of VC^+ is of $^1\Delta(1)$ symmetry and can be thought of as originating from the 'ground' $X\ ^3\Delta(1)$ state after a spin flip of the symmetry-carrying $\delta_\pm$ electron. Indeed, the wavefunction, as well as the atomic populations are practically similar between these two states (table 3). Since no singlets can be formed from the ground state atomic fragments, the $2\ ^1\Delta(1)$ state arises from the excited $V^+(4s^13d^3,\ a\ ^3F) + C(^3P)$ channel, altering similarly its character to $V^+(3d^4,\ a\ ^3P) + C(^3P)$ due to an avoided crossing after ~ 5 bohr towards the equilibrium distance. The adiabatic binding energy at the MRCI (MRCI + Q) level of theory is 95.5(96.4) kcal mol^{-1} at a bond length of 1.718(1.72) Å.

About 12 kcal mol^{-1} higher than the $X\ ^3\Delta(1)$ state we find two practically degenerate states, $3\ ^3\Phi(1)$ and $4\ ^3\Pi(1)$, both stemming from the ground state asymptotic fragments $V^+(3d^4,\ a\ ^5D) + C(^3P)$ via the interaction of the $M = \pm 2,\ \pm 1$ and $\pm 2, \mp 1$ components. Their similarities are reflected in the wavefunction composition and atomic populations in table 3. Bonding comprises 2½ bonds (one σ and 3/2 π) as indicated in the following vbL scheme:

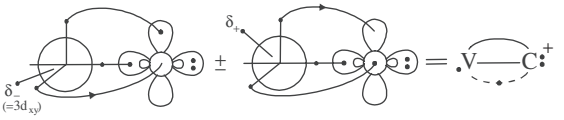

$V^+(3d^4, {}^5D;\ M = \pm 2)$ C (^3P; $M = \pm 1$ or ∓ 1) $3\ ^3\Phi(1)$ or $4\ ^3\Pi(1)$ (3)

The binding energy and bond length in both states amount to ~67 kcal mol^{-1} and ~1.74 Å, respectively. The V atom gains ~0.3 e^- through the σ bonding frame, while returning ~0.4 e^- via the π skeleton (table 4), in accordance with the observed Mulliken charge, $q_V = +1.11$.

The $M = \pm 1, 0$ combination of the same asymptotic limit produces the highly excited *13* $^3\Pi(2)$ state after an avoided crossing with the aforementioned *4* $^3\Pi(1)$ state near $r_{V\text{-}C} \approx 4.5$ bohr. Using the data of table 3, the following bonding scenario obtains for the *13* $^3\Pi(2)$ state, the two atoms being connected with one less σ electron than in the 4 $^3\Pi(1)$ state.

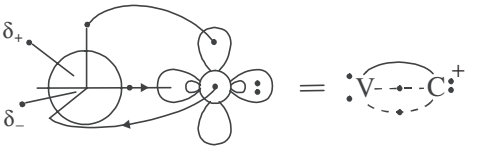

$V^+(3d^4, {}^5D;\ M = \pm 1)$ C (^3P; $M = 0$) *13* $^3\Pi(2)$ (4)

Table 4. Comparison of total energies E (hartree), dissociation energies D_e (kcal mol^{-1}), bond lengths r_e (Å) , and $1\ ^1\Sigma^+ \leftarrow X\ ^3\Delta$ energy separation T_e (kcal mol^{-1}) of the competing $^3\Delta$ and $^1\Sigma^+$ states of VC^+ at increasing levels of theory.

	$VC^+(X^3\Delta)$			$VC^+(1\ ^1\Sigma^+)$			
Method	E	D_e[a]	r_e	E	D_e[b]	r_e	T_e
CASSCF	−980.48918	70.32	1.670	−980.49289	88.5	1.569	−2.33
MRCI	−980.63340	79.02	1.667	−980.62853	100.1	1.576	3.06
MRCI + Q	−980.6408	79.38	1.670	−980.6361	100.9	1.583	2.95
MRCI(DK)	−985.89415	82.83	1.664	−985.89117	101.5	1.573	1.87
MRCI + Q(DK)	−985.9017	83.32	1.667	−985.8986	101.8	1.580	1.95
C-MRCI	−980.94149	83.02	1.648	−980.93554	106.9	1.562	3.73
C-MRCI + Q	−980.9807	84.84	1.651	−980.9729	108.3	1.567	4.89
ZPE(C-MRCI)		−1.31			−1.45		
BSSE(MRCI)		−0.16			−0.18		
Best value		85.4[c]	1.645		106.5[c]	1.559	2.7[d]
'Shifted' value[e]							1.6

[a] Dissociation energy with respect to $V^+(a\ ^5D) + C(^3P)$.
[b] Dissociation energy with respect to $V^+(a\ ^3P) + C(^3P)$.
[c] $D_0\ (= D_e - \omega_e/2)$ value, see text for details; the experimental value is $D_0 = 88.4 \pm 1.2$ kcal mol^{-1} [5b].
[d] Zero-point-corrected energy separation, $T_0 = T_e - \Delta\omega_e/2$.
[e] Value corrected due to the calculational error of the $V^+\ a\ ^3P \leftarrow a\ ^5D$ gap.

A spin flip in the *3* $^3\Phi(1)$ and *4* $^3\Pi(1)$ states gives the corresponding *5* $^1\Phi(1)$ and *7* $^1\Pi(1)$ singlets. The wavefunctions as well as the charge distributions (table 3) show the remarkable similarity between the Φ states, while some differences begin to appear between the Π states due to the active participation of more configurations in the wavefunction of the *7* $^1\Pi(1)$ state (table 3). The open-singlet version of scheme 3 gives a rather faithful view of the bonding.

The 6th excited state of VC^+, *6* $^5\Pi(1)$, lies $\sim$22 kcal mol^{-1} above the ground $X\ ^3\Delta$ state (table 2). This state starts at infinity from $V^+(a\ ^5D;\ M=\pm2) + C(^3P;\ M=\mp1)$, but not far from the equilibrium distance ($\sim$4.5 bohr) suffers an avoided crossing with a state of the same symmetry, *14* $^5\Pi(2)$, coming from the $M=0,\pm1$ components of the same dissociation channel. Due to their mutual interaction, these two states, *6* $^5\Pi(1)$ and *14* $^5\Pi(2)$, show significant multireference character at equilibrium (table 3). A high-spin version of scheme 4 can be utilized to interpret qualitatively the bonding in the *6* $^5\Pi(1)$ state, while for *14* $^5\Pi(2)$ we can attempt to draw the following icon:

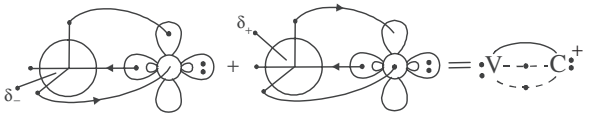

(5)

$V^+(3d^4, {}^5D;\ M=\pm2)$ C ($^3P;\ M=\mp1$) *14* $^5\Pi(2)$

The V atom practically maintains the +1 charge at the equilibrium bond distance.

Next in ascending energy order we find three consecutive states of Σ^+ symmetry. The *8* $^5\Sigma^+(1)$ state is produced by the $V^+(a\ ^5D;\ M=\pm1) + C(^3P;\ M=\mp1)$ reactants and is in conformity with vbL icon 6

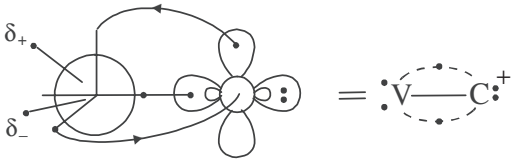

(6)

$V^+(3d^4, {}^5D;\ M=\pm1)$ C ($^3P;\ M=\mp1$) *8* $^5\Sigma^+(1)$

indicating that *8* $^5\Sigma^+(1)$ can be considered to originate from the *6* $^5\Pi(1)$ state by transferring a π electron to a σ orbital. The electronic charge distribution (table 3) reveals that in equilibrium, V has donated to carbon about 0.3 π e$^-$, but has received approximately 0.2 σ e$^-$ resulting in an overall charge of +1.10 on V. The binding energy and bond length in this state are $D_e = 53.1$ kcal mol^{-1} and $r_e = 1.891$ Å, respectively (MRCI level, table 2).

Now, a spin flip of a π or a δ electron in the *8* $^5\Sigma^+$ state essentially creates the 9 $^3\Sigma^+(1)$ state. The similarity between the two states is reflected in their wavefunction compositions and atomic Mulliken distributions (table 3). As a result of the spin flip, the bond becomes weaker by 6–7 kcal mol^{-1} and longer by about 0.025 Å (table 2).

A spin decoupling of the σ bond in the *8* $^5\Sigma^+(1)$ state gives the third Σ^+ state, *10* $^7\Sigma^+(1)$, 33.2 (32.5) kcal mol^{-1} above the $X^3\Delta$ state at the MRCI(MRCI + Q) level:

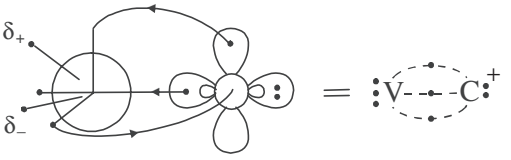

(7)

$V^+(3d^4, {}^5D;\ M=\pm1)$ C ($^3P;\ M=\mp1$) *10* $^7\Sigma^+(1)$

The equilibrium wavefunction is dominated by a single configuration ($C_0 = 0.97$, table 3) as expected due to its high-spin character. Two δ electrons are localized on V while we observe a 0.45 σ e$^-$ C-to-V transfer, with a synchronous V-to-C π–backtransfer of about 0.5 e$^-$ (table 3). The bond has a similar strength to the one in the 9 $^3\Sigma^+(1)$ state, but with a length about one-tenth of an Å longer (2.001 versus 1.915 Å, MRCI level, table 2).

The leading configuration of the *15* $^7\Pi(1)$ state is produced by the $3\sigma^1 \rightarrow 2\pi^1$ promotion of the *10* $^7\Sigma^+(1)$ state. The wavefunction though is much more complex owing to its multireference character (table 3). Dissociation to its adiabatic $V^+(^5D) + C(^3P)$ products requires 32.5(34.5) kcal mol^{-1}. The $|1\sigma^2 2\sigma^1 3\sigma^1 1\pi^2 2\pi^1 1\delta^1|$ determinant, which contributes actively in the *15* $^7\Pi(1)$ state, is the dominant component of the *16* $^7\Phi(1)$ state (table 3), the highest VC^+ excited state studied in the present work ($T_e = 46.7$ kcal mol^{-1}, table 2). It also has the largest equilibrium bond distance ($r_e = 2.075$ Å) and the smallest bond strength ($D_e = 32.5$ kcal mol^{-1}), with respect to its asymptotic products $V^+(^5D) + C(^3P)$ at the MRCI level of theory. The bond can be described by vbL icon 8:

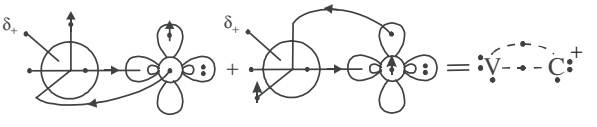

(8)

$V^+(4s^1 3d^3, {}^5F;\ M=\pm3)$ C ($^3P;\ M=0$) *16* $^7\Phi(1)$

The $M = (\pm3, 0)$ character of V and C in the equilibrium of the 16 $^7\Phi(1)$ state is not maintained along the dissociation coordinate due to an avoided crossing near 4.5 bohr with an incoming $^7\Phi$ state correlating to the $V^+(a\ ^5D;\ M=\pm2) + C(^3P;\ M=\pm1)$ fragments.

Coupling of the 2π electron of the *16* $^7\Phi(1)$ state with the 1π electron into a singlet, creates the leading configuration in the wavefunction of the *11* $^5\Phi(1)$ state (see scheme 8). As a result, the population distributions are quite similar (table 3). V and C are held together by ½ σ and 1½ π bonds, with an MRCI(MRCI + Q) binding energy of $D_e = 45.1$ (46.6) kcal mol^{-1} at $r_e = 1.901(1.908)$ Å.

Finally, the *12* $^5\Delta(1)$ state lies 34.3 kcal mol^{-1} above the ground state and at equilibrium it can be well represented by the $1\sigma^2 2\sigma^1 1\pi^3 2\pi^1 1\delta^1$ configuration (table 3). We encountered some technical difficulties while calculating its potential energy curve due to its significant interaction with the higher (not calculated) $^5\Delta(2)$ state near 4.4 bohr. The *12* $^5\Delta(1)$ state is the state where vanadium obtains its higher charge at the equilibrium bond distance, $q_V = +1.20$. The bond can be succinctly envisaged with the following scheme

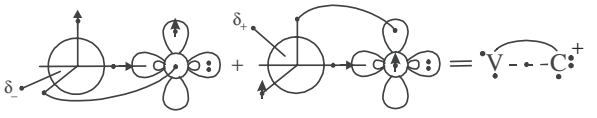

(9)

$V^+(3d^4, {}^5D; M = \pm 2)$ C (^{3}P; M = 0) *12* $^5\Delta(1)$

The MRCI binding energy and bond length are $D_e = 44.9$ kcal mol^{-1} and $r_e = 1.928$ Å.

3.2 *The CrC$^+$ cation*

Table 5 lists our numerical results for all 19 computed states of the CrC^+ cation, while table 6 gives the asymptotic descriptions $|Cr^+>|C>$, leading CASSCF equilibrium configurations, and CASSCF Mulliken atomic populations. Full potential energy curves at the MRCI level are shown in figure 2.

Our recent MRCI calculations [9] have indicated, similarly to VC^+, that a ground state antagonism is also found between the $^2\Delta(1)$ and $^4\Sigma^-(1)$ states. The $^4\Sigma^-(1)$ state springs from the ground state fragments $Cr^+(^6S,\ 3d^5) + C(^3P)$ and exhibits a rather 'smooth' potential energy curve (figure 2). The bonding is clearly represented by the following vbL icon featuring two π and 1/2 σ bonds.

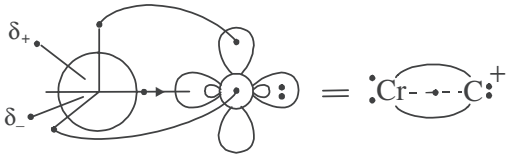

(10)

$Cr^+(3d^5, {}^6S)$ C (^{3}P; M = 0) $^4\Sigma^-$

On the other hand, the $^2\Delta(1)$ state dissociates adiabatically to the excited $Cr^+(4s^1 3d^4,\ a\ ^4D) + C(^3P)$ channel, but the wavefunction composition along the potential energy curve, and especially at equilibrium (table 5), indicates that diabatically the $^2\Delta(1)$ state comes from an even higher dissociation channel, namely $Cr^+(3d^5,\ a\ ^4G) + C(^3P)$. The resulting avoided crossing is reflected in the 'break' observed in the potential energy curve of the $^2\Delta(1)$ state (figure 2). The bonding at equilibrium suggests a similarity with the other competing state in VC^+, $^1\Sigma^+(1)$; indeed, both states are triply bonded.

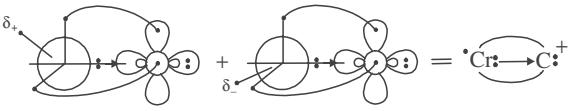

(11)

$Cr^+(3d^5, {}^4G; M = \pm 2)$ C (^{3}P; M = 0) $^2\Delta$

The formal ground state of CrC^+ at the MRCI level of theory is the $^4\Sigma^-$ state, as also indicated by the limited MRCI calculations of Harrison [12] and by the B3LYP and BPW91 results of Gutsev *et al.* [13]. The latter authors have also pointed out the existence of a $^2\Delta$ state lying 3.69(B3LYP) or 1.34(BPW91) kcal mol^{-1} above the $^4\Sigma^-$ state. Moreover, at the BLYP level, $^2\Delta$ becomes the ground state by just 0.76 kcal mol^{-1}, however, nothing is mentioned about its binding mode [13]. As the results of table 7 indicate, inclusion of Douglas–Kroll relativistic effects as well as core/valence contributions renders $^2\Delta$ the ground state of CrC^+, with the $^4\Sigma^-$ lying 2.3 kcal mol^{-1} higher [9]. It is notable that the main factor responsible for the larger stabilization of $^2\Delta$ vs $^4\Sigma^-$ is the effect of the $3s^2 3p^6$ electron 'core' correlation of Cr. A further widening of the energy gap between these two states is produced by a curve shift to match the dissociation channels' experimental energy gap, as done before in the VC^+ case (*vide supra*). Keeping in mind the *in situ* ^{4}G character of Cr^+ in the $^2\Delta$ state, 'perfect' parallel curve shifting furnishes an upper limit of $T_0(^4\Sigma^- \leftarrow {}^2\Delta) = 6.8$ kcal mol^{-1}. Thus, we feel quite certain that the ground state of CrC^+ is $^2\Delta$ rather than $^4\Sigma^-$ with the latter lying at least 3 kcal mol^{-1} higher.

Indirect evidence of the $^2\Delta$ rather than $^4\Sigma^-$ ground state character of CrC^+ is provided by Zhang and coworkers' available experimental dissociation energy [6] of $D_0 = 66.2 \pm 5.8$ kcal mol^{-1}: our best D_0 value for the $^4\Sigma^-$ state including core/valence correlation and DK relativistic effects is no more than 53.5 kcal mol^{-1} (cf. with the 1986 limited MRCI/DZ value of 31.5 kcal mol^{-1}) [12]. As our experience with ScC^+, TiC^+, and VC^+ indicates [9, 10] this value should fall short to an experimental value by about 2–3 kcal mol^{-1} due to the basis set incompleteness. The final $D_0(^4\Sigma^-)$ value would then equal to about 56 kcal mol^{-1}, still lower from the experiment by maybe about 10 kcal mol^{-1}.

Table 5. Total energies E (hartree), dissociation energies D_e (kcal mol^{-1}), bond lengths, r_e (Å), harmonic and anharmonic frequencies ω_e, $\omega_e x_e$ (cm^{-1}), and energy gaps T_e (kcal mol^{-1}) of nineteen states of the CrC^+ species at the MRCI[a] (MRCI + Q)[b] level of theory.

State[c]	$-E$	D_e[d]	r_e	ω_e	$\omega_e x_e$	T_e
$X\,^2\Delta(1)$	1081.07817	106.0	1.582	918	4.8	0.0
	(0.0881)	(106.9)	(1.59)	(908)	(6.4)	
$1\,^4\Sigma^-(1)$	1081.07852	46.2	1.660	825	6.8	−0.22
	(0.0889)	(47.4)	(1.66)	(817)	(7.0)	(−0.50)
$2\,^4\Pi(1)$	1081.06583	41.8	1.759	696	4.4	7.7
	(0.0792)	(40.8)	(1.76)	(678)	(9.0)	(5.6)
$3\,^2\Sigma^-(1)$	1081.05676	91.8	1.711	1015		13.4
	(0.0675)	(93.2)	(1.72)	(1004)		(12.9)
$4\,^6\Pi(1)$	1081.04185	23.4	1.942	671	37	22.8
	(0.0542)	(25.6)	(1.94)	(685)	(32)	(21.3)
$5\,^2\Pi(1)$	1081.03829	80.5	1.755	718	7.7	25.0
	(0.0497)	(82.4)	(1.76)	(715)	(7.9)	(24.1)
$6\,^6\Sigma^-(1)$	1081.03797	20.9	1.893	651	2.5	25.2
	(0.0496)	(22.8)	(1.89)	(647)	(4.4)	(24.2)
$7\,^8\Pi(1)$	1081.02755	14.4	2.090			31.8
	(0.0400)	(16.7)	(2.11)			(30.2)
$8\,^4\Delta(1)$	1081.02349	50.6	1.776	772	4.6	34.3
	(0.0356)	(53.7)	(1.78)	(761)	(8.1)	(32.9)
$9\,^6\Sigma^+(1)$	1081.02257	40.8	1.984	569	31	34.9
	(0.0347)	(42.4)	(1.99)	(566)	(28)	(33.5)
$10\,^2\Gamma(1)$	1081.01991		1.639	930	7.8	36.6
	(0.0311)		(1.64)	(917)	(6.3)	(35.8)
$11\,^8\Sigma^-(1)$	1081.01334	5.3	2.048	627	27	40.7
	(0.0252)	(7.4)	(2.06)	(574)	(32)	(39.5)
$12\,^2H(1)$	1081.00907		1.692	849	4.1	43.4
	(0.0206)		(1.70)	(839)	(5.4)	(42.4)
$13\,^6\Pi(2)$	1081.00165	28.1	1.963	699	8.6	48.0
	(0.0168)	(31.4)	(1.95)	(702)	(7.2)	(44.7)
$14\,^4\Pi(2)$	1081.00029	35.9	1.942	652		48.9
	(0.0139)	(40.0)	(1.94)	(672)		(46.6)
$15\,^6\Delta(1)$	1080.99498	23.7	1.867	727		52.2
	(1081.0096)	(26.9)	(1.87)	(723)		(49.3)
$16\,^4\Phi(1)$	1080.99106	30.2	1.852	500	16	54.7
	(1081.0038)	(33.5)	(1.85)	(502)	(3.6)	(52.9)
$17\,^4\Pi(3)$	1080.99001	29.7	1.879	499	14	55.3
	(1081.0033)	(33.0)	(1.87)	(532)	(12)	(53.2)
$18\,^4\Sigma^+(1)$	1080.98083	23.8	2.212	284	5.4	61.1
	(0.9917)	(26.2)	(2.17)	(336)	(2.2)	(60.5)

[a]Internally contracted MRCI.
[b]'+Q' refers to the multireference Davidson correction.
[c]Numbers in parenthesis after the term symbol indicate the ordering according to energy within the same symmetry manifold.
[d]D_e with respect to the adiabatic products.

On the other hand, our best adiabatic dissociation energy of the $^2\Delta$ state with respect to the $Cr^+(a\,^4D) + C(^3P)$ atoms is 111.1 kcal mol^{-1}. Since the experimental D_0 result refers to the ground state $Cr^+(a\,^6S) + C(^3P)$ channel, the final D_0 value of the $^2\Delta$ state becomes at least $56 + T_0(^4\Sigma^- \leftarrow {}^2\Delta) \approx 59$ kcal mol^{-1}, a value approaching the experimental result, indicating also the difficulty in determining the ground state of CrC^+.

Table 6. Asymptotic fragments, leading equilibrium CASSCF CFs, and equilibrium CASSCF Mulliken atomic populations of nineteen CrC^+ states.

			Equilibrium CASSCF Mulliken atomic populations										
			Cr							C			
State	Adiabatic fragments[a]	Dominant equilibrium CASSCF CFs	4s	$4p_\sigma$	$4p_\pi$	$3d_\sigma$	$3d_{xz}$	$3d_{yz}$	$3d_\delta$	2s	$2p_z$	$2p_x$	$2p_y$
$X\,^2\Delta(1)$	$\|\pm1\rangle\|\pm1\rangle$[d]	$0.88\|1\sigma^2 2\sigma^2 1\pi_x^2 1\pi_y^2 1\delta^1\rangle$	0.15	0.10	0.06	1.29	1.18	1.18	1.0	1.76	0.69	0.77	0.77
$1\,^4\Sigma^-(1)$	$\|0\rangle\|0\rangle$	$0.85\|1\sigma^2 2\sigma^1 1\pi_x^2 1\pi_y^2 1\delta_+^1 1\delta_-^1\rangle$	0.09	0.07	0.04	0.68	1.05	1.05	2.0	1.72	0.45	0.90	0.90
$2\,^4\Pi(1)$	$\|0\rangle\|\pm1\rangle$	$0.79\|1\sigma^2 2\sigma^2 1\pi_x^2 1\pi_y^1 1\delta_+^1 1\delta_-^1\rangle$[g]	0.15	0.05	0.04	1.05	1.01	0.60	2.0	1.82	0.90	0.93	0.40
$3\,^2\Sigma^-(1)$	$\|\pm1\rangle\|\mp1\rangle$[d]	$0.65\|1\sigma^2 2\sigma^1 1\pi_x^2 1\pi_y^2 1\delta_+^1 1\delta_-^1\rangle$ $-0.32\|1\sigma^2 2\sigma^1 1\pi_x^2 1\pi_y^2(1\delta_+^1 1\delta_-^1 + 1\delta_+^1 1\delta_-^1)\rangle$	0.12	0.07	0.04	0.45	1.13	1.13	2.0	1.60	0.78	0.83	0.83
$4\,^6\Pi(1)$	$\|0\rangle\|\pm1\rangle$	$0.70\|1\sigma^2 2\sigma^1 3\sigma^1 1\pi_x^2 1\pi_y^1 1\delta_+^1 1\delta_-^1\rangle$ $+0.42\|1\sigma^2 2\sigma^2 1\pi_x^1 2\pi_x^1 1\pi_y^1 1\delta_+^1 1\delta_-^1\rangle$[g]	0.29	0.08	0.03	0.97	1.00	0.65	2.0	1.77	0.86	0.95	0.36
$5\,^2\Pi(1)$	$\|0\rangle\|\pm1\rangle$[d]	$0.68\|1\sigma^2 2\sigma^2 1\pi_x^2 1\pi_y^1 1\delta_+^1 1\delta_-^1\rangle - 0.39\|1\sigma^2 2\sigma^2 1\pi_x^2 1\pi_y^1 1\delta_+^1 1\delta_-^1\rangle$[g]	0.15	0.10	0.05	1.18	1.12	0.31	2.0	1.76	0.80	0.82	0.68
$6\,^6\Sigma^-(1)$	$\|0\rangle\|0\rangle$	$0.59\|1\sigma^2 2\sigma^1(1\pi_x^1 2\pi_x^1 1\pi_y^2 + 1\pi_x^2 1\pi_y^1 2\pi_y^1)1\delta_+^1 1\delta_-^1)\rangle$	0.12	0.08	0.06	0.50	1.05	1.05	2.0	1.69	0.62	0.90	0.90
$7\,^8\Pi(1)$	$\|0\rangle\|\pm1\rangle$	$0.98\|1\sigma^2 2\sigma^1 3\sigma^1 1\pi_x^1 2\pi_x^1 1\pi_y^1 1\delta_+^1 1\delta_-^1\rangle$[g]											
$8\,^4\Delta(1)$	$\|\pm1\rangle\|\pm1\rangle$[d]	$0.71\|1\sigma^2 2\sigma^1 3\sigma^1 1\pi_x^2 1\pi_y^2 1\delta_+^1\rangle$[f]	0.51	0.05	0.04	0.97	1.16	1.26	1.0	1.68	0.77	0.80	0.80
$9\,^6\Sigma^+(1)$	$\|0\rangle\|0\rangle$[b]	$0.90\|1\sigma^2 2\sigma^2 3\sigma^1 1\pi_x^1 1\pi_y^1 1\delta_+^1 1\delta_-^1\rangle$	0.60	0.05	0.02	1.05	0.68	0.68	2.0	1.89	1.33	0.33	0.33
$10\,^2\Gamma(1)$	[e]	$0.63\|1\sigma^2 2\sigma^1 1\pi_x^2 1\pi_y^2(1\delta_+^2 - 1\delta_-^2)\rangle$[f]	0.10	0.07	0.04	0.59	1.09	1.09	2.0	1.68	0.57	0.86	0.86
$11\,^8\Sigma^-(1)$	$\|0\rangle\|0\rangle$	$0.99\|1\sigma^2 2\sigma^1 1\pi_x^1 2\pi_x^1 1\pi_y^1 2\pi_y^1 1\delta_+^1 1\delta_-^1\rangle$	0.22	0.10	0.08	0.37	1.01	1.01	2.0	1.66	0.65	0.94	0.94
$12\,^2\mathrm{H}(1)$	$\|\pm4\rangle\|\pm1\rangle$[e]	$0.55\|1\sigma^2 2\sigma^2 1\pi_x^2 1\pi_y^1 1\delta_+^1 1\delta_-^1\rangle - 0.45\|1\sigma^2 2\sigma^2 1\pi_x^1 1\pi_y^2(1\delta_+^2 - 1\delta_-^2)\rangle$[g]	0.12	0.09	0.04	1.16	0.77	0.77	2.0	1.79	0.82	0.69	0.69
$13\,^6\Pi(2)$	$\|0\rangle\|\pm1\rangle$[b]	$0.73\|1\sigma^2 2\sigma^2 1\pi_x^1 2\pi_x^1 1\pi_y^1 1\delta_+^1 1\delta_-^1\rangle$ $-0.46\|1\sigma^2 2\sigma^2 3\sigma^1 1\pi_x^2 1\pi_y^1 1\delta_+^1 1\delta_-^1\rangle$[g]	0.20	0.06	0.03	0.94	0.99	0.75	2.0	1.85	0.92	0.97	0.26
$14\,^4\Pi(2)$	$\|0\rangle\|\pm1\rangle$[c]	$0.43\|1\sigma^2 2\sigma^1 3\sigma^1 1\pi_x^2 1\pi_y^1 1\delta_+^1 1\delta_-^1\rangle$ $-0.26\|1\sigma^2 2\sigma^2 1\pi_x^2 2\pi_y^1 1\delta_+^1 1\delta_-^1\rangle$ $-0.25\|1\sigma^2 2\sigma^2 1\pi_x^1 1\pi_x^1 1\pi_y^1 1\delta_+^1 1\delta_-^1\rangle$[g]	0.52	0.05	0.03	0.91	1.08	0.48	1.82	1.75	0.91	0.80	0.60
$15\,^6\Delta(1)$	$\|0\rangle\|\pm2\rangle$[b]	$0.63\|1\sigma^2 2\sigma^1(1\pi_x^1 1\pi_y^2 2\pi_y^1 - 1\pi_x^2 2\pi_x^1 1\pi_y^1)1\delta_+^1 1\delta_-^1)\rangle$[f]	0.11	0.07	0.06	0.56	1.05	1.05	2.0	1.75	0.54	0.90	0.90
$16\,^4\Phi(1)$	$\|\pm2\rangle\|\pm1\rangle$[c]	$0.56\|1\sigma^2 2\sigma^2 3\sigma^1(1\pi_x^1 1\pi_y^2 1\delta_+^1 + 1\pi_x^2 1\pi_y^1 1\delta_-^1)\rangle$[g]	0.67	0.05	0.02	1.21	1.00	1.00	1.06	1.87	1.09	0.49	0.49
$17\,^4\Pi(3)$	$\|\pm2\rangle\|\mp1\rangle$[c]	$0.47\|1\sigma^2 2\sigma^2 3\sigma^1(1\pi_x^1 1\pi_y^2 1\delta_+^1 - 1\pi_x^2 1\pi_y^1 1\delta_-^1)\rangle$[g]	0.61	0.05	0.03	1.13	1.01	0.85	1.30	1.83	1.03	0.61	0.51
$18\,^4\Sigma^+(1)$	$\|\pm1\rangle\|\mp1\rangle$[c]	$\|1\sigma^2 2\sigma^2 3\sigma^1(-0.39(1\pi_x^1 1\pi_y^1) - 0.27(1\pi_x^1 1\pi_y^1))1\delta_+^1 1\delta_-^1\rangle$ $+\|1\sigma^2 2\sigma^2 3\sigma^1(0.37(2\pi_x^1 1\pi_y^1) - 0.34(1\pi_x^1 2\pi_y^1))1\delta_+^1 1\delta_-^1\rangle$	0.95	0.06	0.00	1.04	0.51	0.51	2.0	1.89	1.00	0.50	0.50

[a] $|Cr^+;{}^6S;M\rangle|C;{}^3P;M\rangle$.
[b] $|Cr^+;{}^6S;M\rangle|C;{}^1D;M\rangle$.
[c] $|Cr^+;{}^6D;M\rangle|C;{}^3P;M\rangle$.
[d] $|Cr^+;{}^4D;M\rangle|C;{}^3P;M\rangle$.
[e] $|Cr^+;{}^4G;M\rangle|C;{}^3P;M\rangle$.
[f] A_1 symmetry component.
[g] B_1 symmetry component.

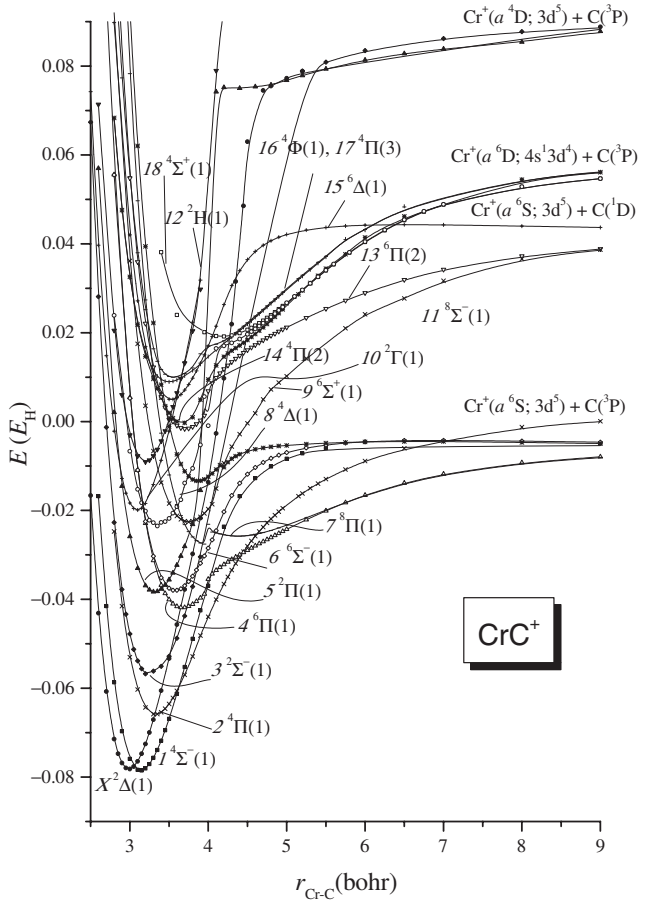

Figure 2. Potential energy curves of CrC^+. MRCI level of theory.

This is a rather eloquent demonstration of the fact that one should always have in mind the atomic fragment origin of each molecular state for a correct interpretation of the computational results.

The ground $Cr^+(a\ ^6S) + C(^3P)$ dissociation channel produces also a $^4\Pi$ state, the second excited state of CrC^+ ($T_e = 7.7$ kcal mol^{-1}, MRCI level). A σ and 3/2 π bonds are formed according to the vbL icon 12:

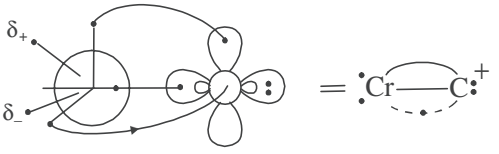

(12)

$Cr^+(3d^5, {}^6S)$ C (^3P; M = ±1) $2\ ^4\Pi(1)$

Similarly to ScC^+, TiC^+, and VC^+ [9, 10], this '1 σ and 3/2 π bond' state ($2\ ^4\Pi$) is higher in energy than the '1/2 σ and 2 π bond' state ($1\ ^4\Sigma^-$) signifying the relevant 'hesitation' of the transition metal atom to form a full σ bond [1]. The binding energy and bond length of the $2\ ^4\Pi(1)$ state are much different than the limited MRCI values of Harrison [12], 41.8 versus 13.4 kcal mol^{-1}, and 1.759 versus 2.059 Å, respectively, indicating the difference in size between the two calculations.

The third excited state of CrC^+, $3\ ^2\Sigma^-(1)$, can be envisaged as created after a spin-flip of an unpaired electron of the $1\ ^4\Sigma^-(1)$ state (scheme 10 and table 6). Like the ground $X\ ^2\Delta$ state, it traces its origin to the excited $Cr^+(4s^13d^4,\ a\ ^4D) + C(^3P)$ channel, suffering

Table 7. Comparison of total energies E (hartree), dissociation energies D_e (kcal mol^{-1}), bond lengths r_e (Å) , and $1\ ^4\Sigma^- \leftarrow X\ ^2\Delta$ energy separation T_e (kcal mol^{-1}) of the competing $^2\Delta$ and $^4\Sigma^-$ states of CrC^+ at increasing levels of theory.

	$CrC^+(X\ ^2\Delta)$			$CrC^+(1\ ^4\Sigma^-)$			
Method	E	D_e[a]	r_e	E	D_e[b]	r_e	T_e
MRCI	−1081.07817	106.0	1.582	−1081.07852	46.22	1.660	−0.22
MRCI + Q	−1081.0881	106.9	1.587	−1081.0889	47.38	1.663	−0.50
MRCI (+1h)[c]	−1081.07973	106.7	1.582	−1081.07974	46.61	1.659	−0.01
MRCI + Q (+1h)[c]	−1081.0897	107.5	1.586	−1081.0902	47.80	1.662	−0.31
MRCI(DK)	−1087.39324	105.9	1.579	−1087.39159	50.42	1.654	1.04
MRCI + Q(DK)	−1087.4034	106.8	1.583	−1087.4021	51.63	1.657	0.82
C-MRCI	−1081.40054	112.2	1.569	−1081.39884	50.39	1.643	1.07
C-MRCI + Q	−1081.4431	114.7	1.573	−1081.4415	53.55	1.647	1.00
ZPE(C-MRCI)	–	−1.40	–	–	−1.26	–	–
BSSE(MRCI)	–	−0.34	–	–	−0.23	–	–
Best value	–	111.1[d]	1.566	–	53.5[d]	1.636	2.3[e]

[a]Dissociation energy with respect to $Cr^+(a\ ^4D)$ + C (^3P).
[b]Dissociation energy with respect to $Cr^+(a\ ^6S)$ + C (^3P).
[c]Values obtained adding one h function (exponent = 1.0) to the Cr basis set.
[d]D_0 ($= D_e - \omega_e/2$) value, see text for details; the experimental value is $D_0 = 66.2 \pm 5.8$ kcal mol^{-1} [6].
[e]Zero-point-corrected energy separation, $T_0 = T_e - \Delta\omega_e/2$.

as well an avoided crossing with a higher $^2\Sigma^-$ state, resulting in a $Cr^+(3d^5, a\ ^4G)$ character at the equilibrium bond distance (*vide supra*). A state with the same ^4D-to-^4G Cr^+ character change is the $5\ ^2\Pi(1)$ state which can be thought of as produced from the $3\ ^2\Sigma^-(1)$ state after moving a π electron to a σ orbital of CrC^+ (table 6). These two states exhibit bonding similarities with the corresponding quartets, $1\ ^4\Sigma^-(1)$ and $2\ ^4\Pi(1)$ favouring energetically the creation of π vs σ bonds (schemes 10 and 12). The binding energy of the $3\ ^2\Sigma^-(1)$ state is 91.8 kcal mol^{-1} with respect to its adiabatic products (table 5), with the 'intrinsic' bond strength (to the diabatic product limit) approaching 96 kcal mol^{-1}. Analysis of the binding mode indicates a 0.35 e^- $Cr^+ \rightarrow C$ σ transfer, along with a 0.30 e^- π backtransfer. On the other hand, the binding energy of the $5\ ^2\Pi(1)$ state is lower by approximately 11 kcal mol^{-1} (table 5).

The first state of sextet spin multiplicity, $4\ ^6\Pi(1)$) is derived from the $2\ ^4\Pi(1)$ state following a σ-frame $2\sigma^2 \rightarrow 2\sigma^1 3\sigma^1$ spin decoupling. This sextet interacts strongly with the higher $13\ ^6\Pi(2)$ state resulting in increased multireference character at their equilibrium distances (table 6). The *in situ* C atom in the $13\ ^6\Pi(2)$ is in the excited ^1D state. The participation of two leading configurations in both states (table 6) is depicted in the following vbL icon

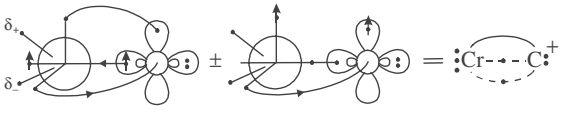

(13)

$Cr^+(3d^5, {}^6S)$ C (^3P; M = ±1 or ^1D; M = ±1) $4\ ^6\Pi(1)$ or $13\ ^6\Pi(2)$

The CASSCF equilibrium coefficients for these two configurations have the values 0.70 and 0.42 [$4\ ^6\Pi(1)$], and −0.46 and 0.73 [$13\ ^6\Pi(2)$]. A 'balanced' mutual charge exchange is observed, resulting to practically zero net electron transfer between the two fragments Cr^+ and C (table 6).

Further electron-pair decoupling, but now in the π-frame, $1\pi^2 \rightarrow 1\pi^1 2\pi^1$, leads to the $7\ ^8\Pi(1)$ state (table 6), which regardless of its high spin multiplicity, has an appreciable bond energy, $D_e = 14.4$ kcal mol^{-1} (MRCI level, table 5). This intrinsically single-reference state can be represented faithfully by the vbL icon with Cr^+ and C interacting through a half σ and a half π bond.

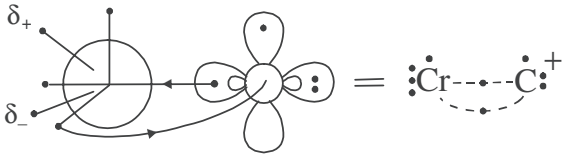

(14)

$Cr^+(3d^5, {}^6S)$ C (^3P; M = ±1) $7\ ^8\Pi(1)$

The leading configurations of the $6\ ^6\Sigma^-$ and $11\ 8\Sigma^-(1)$ states can be produced in a similar fashion as before by sequential decoupling of the first ($1\pi_x^2 \rightarrow 1\pi_x^1 2\pi_x^1$) and second ($1\pi_y^2 \rightarrow 1\pi_y^1 2\pi_y^1$) π bonds of the $1\ ^4\Sigma^-(1)$ state, respectively. Both these states exhibit the largest Cr^+-to-C electron transfer observed in the present study (0.13 and 0.22 e^-, respectively), while the 2s orbital of the C atom shows significant 'hybridisation' carrying 1.69 and 1.66 e^- at equilibrium (table 6), as opposed to 1.96 e^- at infinity. They both emerge from the ground state asymptotic limits and can be pictured as follows:

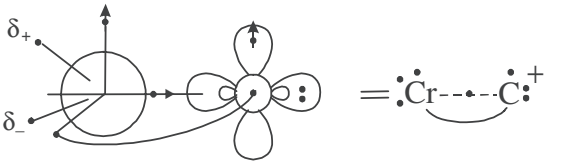

(15)

$Cr^+(3d^5, {}^6S)$ C (^3P; M = 0) $6\ ^6\Sigma^-(1)$

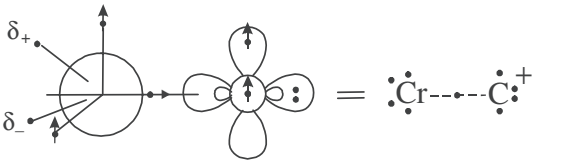

(16)

$Cr^+(3d^5, {}^6S)$ C (^3P; M = 0) $11\ ^8\Sigma^-(1)$

As would be expected, the successive reduction in the number of bonds is accompanied by gradual bond weakening reflected in the binding energies ($D_e = 46.2$ versus 20.9 versus 5.3 kcal mol^{-1}) and the elongation of the bond lengths ($r_e = 1.660$ vs 1.893 vs 2.048 Å), as we move from the quartet to the sextet and to the octet state (MRCI values, table 5).

The lowest-in-energy state stemming from the first excited $Cr^+(4s^1 3d^4, a\ ^6D) + C(^3P)$ channel is the $8\ ^4\Delta(1)$ state. It can be considered as descending from the ground $X\ ^2\Delta(1)$ state after a decoupling of its σ bond. The bonding at equilibrium can be graphically represented by scheme 17.

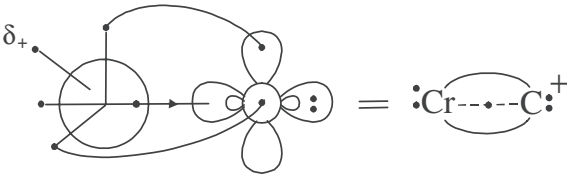

(17)

$Cr^+(4s^1 3d^4, {}^6D;\ M = \pm 2)$ C (^3P; M = 0) $8\ ^4\Delta(1)$

Population analysis shows a ∼0.5 e^- transfer from the 4s orbital of Cr to C, along with a ∼0.4 e^- π backdonation (table 6). The binding energy was found

to be 50.6(53.7) kcal mol^{-1} at the MRCI(MRCI + Q) level of theory.

The opposite bonding situation occurs in the *9* $^6\Sigma^-(1)$ state, where now Cr becomes the σ-'acid' and π-'base'.

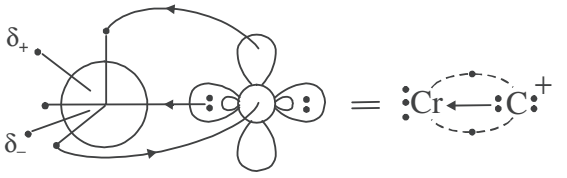

(18)

$Cr^+(3d^5, {}^6S)$ C (^{1}D; M = 0) *9* $^6\Sigma^+(1)$

The characteristic $2p_z^2$ electron distribution of the M = 0 angular momentum component in the first excited state of C(^{1}D) is the driving force of this newly-encountered binding picture, with the +1 charge of Cr becoming slightly quenched ($q_{Cr} = +0.91$), but in a rather 'dynamic' way: carbon offers 0.75 σ electrons while receiving 0.65 in the π skeleton. A similar bonding picture is encountered in the highest excited state of CrC^+ that was studied in the present work, *18* $^4\Sigma^+(1)$, 61.1(60.5) kcal mol^{-1} above the ground state at the MRCI(MRCI + Q) level (table 5). Even though this quartet dissociates to a different asymptotic channel, $Cr^+(4s^13d^4, a\ {}^6D) + C(^3P)$, in equilibrium it can be thought of as coming from the *9* $^6\Sigma^+(1)$ state after a spin flip of an uncoupled π electron (see the rather complicated wavefunction composition of the *18* $^4\Sigma^+(1)$ state in table 6). The observed charge on Cr is again +0.91, but this time it is due to a mere ~0.1 σ e^- transfer from the 2s orbital of C towards Cr; indeed as the Mulliken populations indicate (table 6), π and δ electrons remain localized on the atoms.

The *10* $^2\Gamma(1)$ state is the first one dissociating diabatically to $Cr^+(3d^5, a\ {}^4G) + C(^3P)$. The following bonding scheme conforms with the wavefunction composition as well as the Mulliken charge distribution (table 4):

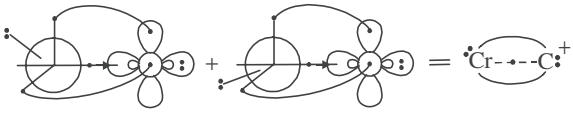

(19)

$Cr^+(3d^5, {}^4G; M = \pm4)$ C (^{3}P; M = 0) *10* $^2\Gamma(1)$

Two π and ½ σ bonds keep together the two atoms in a similar fashion to the bonding in the *1* $^4\Sigma^-(1)$ state. Due to severe technical difficulties we were unable to calculate the full potential energy curve, so the binding energy cannot be accurately calculated for this state. At the MRCI level though, the bond length is equal to 1.639 Å.

The state with the highest angular momentum that was studied in the present work comes from the same asymptotic limit, but with the M = ±4, ±1 components of the $^4G + {}^3P$ atomic levels of Cr^+ and C, respectively. This combination gives a state with $|\Lambda| = 5$, the *12* $^2H(1)$ state. The leading equilibrium determinant has a coefficient of only 0.55, with the next two important determinants multiplied by an even smaller coefficient (0.45, table 6). Despite its highly multireference character, we can attempt to condense its main bonding characteristics in the following vbL icon:

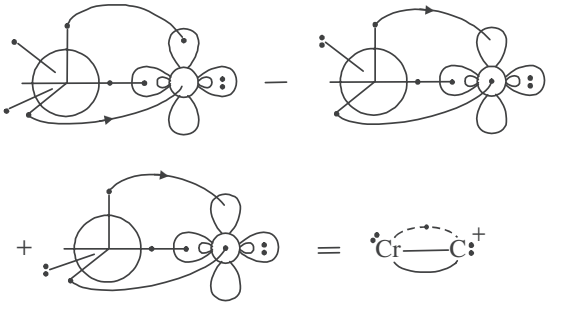

(20)

$Cr^+(3d^5, {}^4G; M = \pm4)$ C (^{3}P; M = ±1) *12* $^2H(1)$

The σ bond is somewhat polarized, Cr earning ~0.4 e^-, with a concomitant π backdonation to C of the same magnitude (table 6). As with the aforementioned *10* $^2\Gamma(1)$ state, a rather short equilibrium bond length is calculated, $r_e = 1.692$ Å at the MRCI level.

The fourteenth excited state of CrC^+ is the second one of $^4\Pi$ symmetry encountered stemming from the $Cr^+(4s^13d^4, a\ {}^6D) + C(^3P)$ fragments. Around 4 bohr it interacts strongly with the incoming $^4\Pi(3)$ state resulting to highly complicated wavefunctions in their equilibrium distances and to difficulty in drawing vbL icons for both states. However, a scheme including the main bonding features of the *17* $^4\Pi(3)$ state would be:

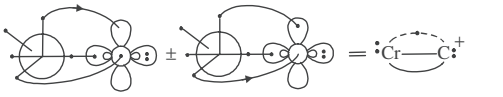

(21)

$Cr^+(4s^13d^4, {}^6D; M = \pm2)$ C (^{3}P; M = ∓1 or ±1) *17* $^4\Pi(3)$ or *16* $^4\Phi(1)$

The '+' sign refers to the *17* $^4\Pi(3)$ state, while the '−' sign to the relevant *16* $^4\Phi(1)$ state. These two states are close to being degenerate as they exhibit a quite similar wavefunction composition as well as energetics and spectroscopic constants (tables 5 and 6). They lie 53.9 and 53.2 kcal mol^{-1} above the ground state at the MRCI level of theory, respectively.

Finally, the last state correlating to the $Cr^+(a\ {}^6S) + C(^1D)$ channel is of $^6\Delta$ symmetry, lying 52.2 kcal mol^{-1} above the ground state. The bonding reflects the

characteristic $p_x^2 - p_y^2$ electron distribution of C(^{1}D, M = ±2), and this can be convincingly pictured in scheme 22:

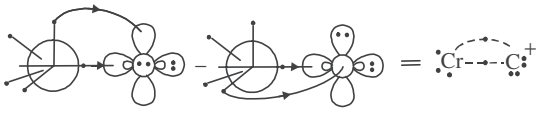

(22)

$Cr^+(3d^5, {}^6S)$ C (^{1}D; M = ±2) $15^6\Delta(1)$

The Cr^+ ion transfers nearly 0.25 e^- to C along the σ skeleton and receives back about 0.15 e^- via its π orbitals, resulting to an observed Mulliken charge on Cr of +1.11. Breaking of this bond in the MRCI(MRCI + Q) level costs 23.7(26.9) kcal mol^{-1} (table 5).

4. Synopsis and remarks

With the intent of studying the low-lying energy spectrum of VC^+ and CrC^+, establishing their ground states, and understanding the bonding milieu, we have presented multireference configuration interaction calculations (MRCI = CASSCF + 1 + 2) using quantitative basis sets. Full potential energy curves were constructed for almost all 36 states (VC^+: 17, CrC^+: 19) and energetics (E, D_e, T_e) along with spectroscopic constants (r_e, ω_e, $\omega_e x_e$) are reported. To the best of our knowledge and apart from the ground states, these are, in essence, the first theoretical results on VC^+ and CrC^+, either theoretical or experimental, to be reported in the literature.

Figures 3 and 4 display a synoptic view of the relative energy levels of the VC^+ and CrC^+ species. Some states are degenerate within the accuracy of our calculations, the most characteristic example being the ground states of both systems. Contrary to those of $ScC^+(X\ ^3\Pi)$ and $TiC^+(X\ ^2\Sigma^+)$, the ground states of VC^+ and CrC^+ are the subject of an intense antagonism between $^3\Delta/^1\Sigma^+$ (VC^+) and $^4\Sigma^-/^2\Delta$ (CrC^+) symmetries. The $^3\Delta$ and $^4\Sigma^-$ states are bonded in a similar fashion as the ground states of ScC^+ and TiC^+, forming two π bonds and a one-electron σ bond (ScC^+ cannot actually form a second two-electron π bond because it is short of one electron). The $^1\Sigma^+$ and $^2\Delta$ states are triply bonded, but although they stem from an excited state of the transition metal cation, they compete in total energy with the former two states because of their significantly higher binding energies. The *in situ* excited state nature of the TM cation in the triply bonded $^1\Sigma^+$ and $^2\Delta$ states introduces a further point of consideration, namely the quantitative description of the relevant atomic level splittings. At our most accurate level of theory, MRCI/MRCI + Q including core/valence $3s^23p^6$ correlation of the transition metal atom, one-electron Douglas–Kroll scalar relativistic effects, basis set superposition errors, zero-point energy corrections, and parallel curve shiftings to correct for the atomic energy separations, the formal ground states of VC^+ and CrC^+ are found to be of $^3\Delta$ and $^2\Delta$ symmetry, respectively. The competing $^1\Sigma^+$ (VC^+) and $^4\Sigma^-$ (CrC^+) states are predicted to be bracketed between 1–3 and 3–7 kcal mol^{-1} higher, depending on the quantitative correctness of the 'perfect' parallel curve shifting. As a result, the $^2\Delta$ ground state identity of CrC^+ appears to be fairly certain, but obviously theory, even at this high level,

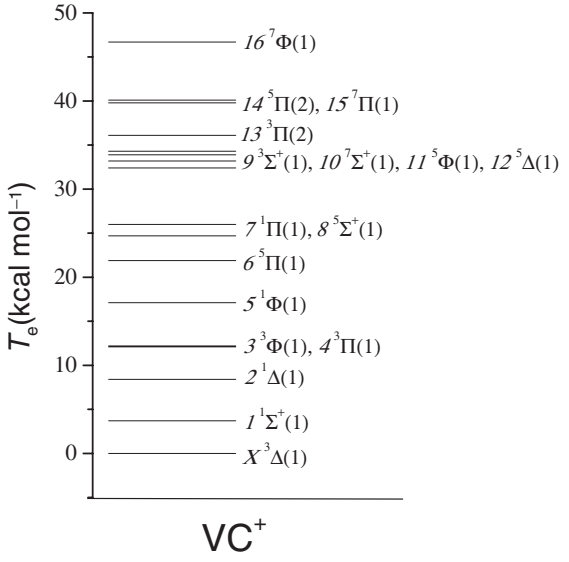

Figure 3. Relative energy levels of the VC^+ states studied. MRCI level of theory.

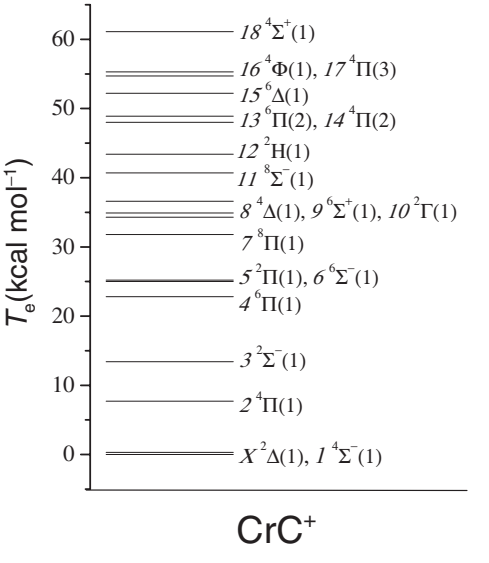

Figure 4. Relative energy levels of the CrC^+ states studied. MRCI level of theory.

cannot give a definitive answer in the case of VC^+. We believe that careful experimental studies on both systems are needed to confirm the symmetry of their ground states.

All 36 states are bound with respect to the ground state atoms $\{V^+(a\ ^5D),\ Cr^+(a\ ^6S)\} + C(^3P)$, with binding energies with respect to their asymptotic fragments ranging from $5.3\,kcal\,mol^{-1}$, *11* $^8\Sigma^-(1)$ (CrC^+) to $111.1\,kcal\,mol^{-1}$, $X\ ^2\Delta$ (CrC^+). The D_0 binding energy of the $X\ ^3\Delta$ state of VC^+ is $85.4\,kcal\,mol^{-1}$, in satisfactory agreement with the experimental value of $88.4 \pm 1.2\,kcal\,mol^{-1}$ [5b]. The estimated binding energy of $CrC^+(X\ ^2\Delta)$ with respect to the ground state atomic fragments verges on the value of $60\,kcal\,mol^{-1}$, in fair agreement with the experimental $D_0 = 66.2 \pm 5.8\,kcal\,mol^{-1}$ [6], while in the competing $^4\Sigma^-$ state, it has an estimated value of $56\,kcal\,mol^{-1}$, indicating, albeit indirectly, the $^2\Delta$ character of the CrC^+ ground state.

A variety of binding modes is observed in the different states of VC^+ and CrC^+. In general, one should point out the synergetic 'donation-backdonation' bonding mechanism noted in many states and along the σ and π bonding frames. Furthermore, in most states studied, a charge transfer up to 0.2 e^- is recorded from the already charged metal cation to the carbon atom. This can be justified by recalling that the ionization potentials of the TM monocations are comparable with that of C. The trend, however, diminishes as we move along the ScC^+, TiC^+, VC^+, CrC^+ direction, owing to the gradual increase in the ionization potential of the TM cation.

Finally, one should comment on the intrinsic complexity of such 'simple' molecular systems due to the multitude of low-lying molecular states which gives rise to potential energy curves of abstruse morphology, the result of avoided curve crossings which, in turn, often cause severe calculational and conceptual difficulties.

Dedicated to Professor Nicholas C. Handy for his outstanding contributions to Quantum Chemistry. The financial support of the National and Kapodistrian University of Athens through its Special Research Account for Basic Research is appreciated.

References

[1] See for instance, Harrison, J. F., 2000, *Chem. Rev.*, **100**, 679, and references therein.

[2] See for instance, Brugh, D. J., and Morse, M. D., 2002, *J. Chem. Phys.*, **117**, 10703, and references therein.

[3] (a) Kalemos, A., Mavridis, A., and Harrison, J. F., 2001, *J. Phys. Chem.* A, **105**, 755. (b) Kalemos, A., and Mavridis, A., 2002, *J. Phys. Chem.* A, **106**, 3905. (c) Tzeli, D., and Mavridis, A., 2002, *J. Chem. Phys.,* **116**, 4901. (d) Tzeli, D., and Mavridis, A., 2003, *J. Chem. Phys.*, **118**, 4984. (e) Kalemos, A., Dunning, T. H., Jr, and Mavridis, A., manuscript to be submitted.

[4] Clemmer, D. E., Elkind, J. L., Aristov, N., and Armentrout, P. B., 1991, *J. Chem. Phys.*, **95**, 3387.

[5] (a) Aristov, N., and Armentrout, P. B., 1986, *J. Am. Chem. Soc.*, **108**, 1806. (b) Armentrout, P. B., and Kickel, B. L., 1996, in *Organometallic Ion Chemistry*, edited by B. S. Freiser (Kluwer Academic Publishers), p. 1.

[6] Qi, F., Sheng, L., Gao, H., Zhang, Y., Yang, X., Yang, S., and Yu, S., 1999, *Chin. J. Chem. Phys.*, **12**, 525.

[7] Hettich, R. L., and Freiser, B. S., 1986, *J. Am. Chem. Soc.,* **108**, 2537.

[8] Haynes, C. L., Chen, Y. M., and Armentrout, P. B., 1995, *J. Phys. Chem.*, **99**, 9110.

[9] Kerkines, I. S. K., and Mavridis, A., 2003, *Collect. Czech. Chem. Commun.*, **68**, 387.

[10] Kerkines, I. S. K., and Mavridis, A., 2000, *J. Phys. Chem.* A, **104**, 11777.

[11] Tzeli, D., and Mavridis, A., manuscript in preparation.

[12] Harrison, J. F., 1986, *J. Phys. Chem.,* **90**, 3313.

[13] Gutsev, G. L., Andrews, L., and Bauschlicher, C. W., Jr., 2003, *Theor. Chem. Acc.,* **109**, 298.

[14] Koga, T., Watanabe, S., Kanayama, K., Yasuda, R., and Thakkar, A. J., 1995, *J. Chem. Phys.,* **103**, 3000.

[15] Bunge, C. F., Barrientos, J. A., Bunge, A. V., and Cogordan, J. A., 1992, *Phys. Rev.* A, **46**, 3691.

[16] Moore, C. E., 1971, *Atomic Energy Levels*, NRSDS-NBS Circular No.35, U.S. GPO: Washington, DC.

[17] Bauschlicher, C. W., Jr., 1995, *Theor. Chim. Acta*, **92**, 183.

[18] Dunning, T. H., Jr., 1989, *J. Chem. Phys.*, **90**, 1007.

[19] (a) Jansen, H. B., and Ros, P., 1969, *Chem. Phys. Lett.*, **3**, 140. (b) Boys, S. F., and Bernardi, F., 1970, *Mol. Phys.*, **19**, 553.

[20] (a) Douglas, M., and Kroll, N. M., 1974, *Ann. Phys. (N. Y.),* **82**, 89. (b) Hess, B. A., 1985, *Phys. Rev.* A, **32**, 756. (c) Hess, B. A., 1986, *Phys. Rev.* A, **33**, 3742.

[21] de Jong, W. A., Harrison, R. J., and Dixon, D. A., 2001, *J. Chem. Phys.*, **114**, 48.

[22] (a) Werner, H.-J., and Knowles, P. J., 1988, *J. Chem. Phys.,* **89**, 5803. (b) Knowles, P. J., Werner, H.-J., and Reinsch, E. A., 1982, *J. Chem. Phys.*, **76**, 3144. (c) Werner, H.-J., 1987, *Adv. Chem. Phys.,* **LXIX**, 1.

[23] (a) Docken, K., and Hinze, J., 1972, *J. Chem. Phys.*, **57**, 4928. (b) Werner, H.-J., and Meyer, W., 1981, *J. Chem. Phys.*, **74**, 5794.

[24] Kalemos, A., and Mavridis, A., 1998, *Adv. Quantum Chem.*, **32**, 69.

[25] MOLPRO a package of *ab initio* programs designed by H.-J. Werner and P. J. Knowles, version 2002.3, R. D. Amos, A. Bernhardsson, A. Berning, P. Celani, D. L. Cooper, M. J. O. Deegan, A. J. Dobbyn, F. Eckert, C. Hampel, G. Hetzer, P. J. Knowles, T. Korona, R. Lindh, A. W. Lloyd, S. J. McNicholas, F. R. Manby, W. Meyer, M. E. Mura, A. Nicklass, P. Palmieri, R. Pitzer, G. Rauhut, M. Schütz, U. Schumann, H. Stoll, A. J. Stone, R. Tarroni, T. Thorsteinsson, and H.-J. Werner.